

Aqueous-Phase Synthesis of Silver Nanodiscs and Nanorods in Methyl Cellulose Matrix: Photophysical Study and Simulation of UV–Vis Extinction Spectra Using DDA Method

Priyanka Sarkar · Dipak Kumar Bhui ·
Harekrishna Bar · Gobinda Prasad Sahoo ·
Sadhan Samanta · Santanu Pyne · Ajay Misra

Received: 13 May 2010/Accepted: 30 June 2010/Published online: 18 July 2010
© The Author(s) 2010. This article is published with open access at Springerlink.com

Abstract We present a very simple and effective way for the synthesis of tunable coloured silver sols having different morphologies. The procedure is based on the seed-mediated growth approach where methyl cellulose (MC) has been used as soft-template in the growth solution. Nanostructures of varying morphologies as well as colour of the silver sols are controlled by altering the concentration of citrate in the growth solution. Similar to the polymers in the solution, citrate ions also dynamically adsorbed on the growing silver nanoparticles and promote one (1-D) and two-dimensional (2-D) growth of nanoparticles. Silver nanostructures are characterized using UV–vis and HR-TEM spectroscopic study. Simulation of the UV–vis extinction spectra of our synthesized silver nanostructures has been carried out using discrete dipole approximation (DDA) method.

Keywords Silver nanostructure · Seed-mediated growth · Methyl Cellulose (MC) · SPR · HR-TEM · Discrete dipole approximation (DDA)

Introduction

Nanoparticles have attracted considerable interest because of their unique optical, electromagnetic, and catalytic properties that differ from bulk ones. The origin of these properties is due to their high surface to volume ratio and the coherent oscillation of the conduction electrons that can be

induced by interactive electromagnetic fields. Properties of nanoparticles are highly size and shape-dependent; therefore, controlled synthesis of nanoparticles in terms of size and shape is a technological scaffold for their potential and fundamental studies.

Particle size distribution, morphology, and surface charge modification play a vital role in determining the optical properties of nanoparticle and there is a growing interest in the controlled synthesis of silver nanoparticles among the all noble metals. Silver has an array of properties that could be tuned through the nanoscale control of morphology. Among all the properties, localized surface plasmon resonance (LSPR) is the most important due to its application in biolabelling [1], surface enhanced Raman scattering (SERS) [2], surface enhanced fluorescence (SEF) [3], sensing [4], and fabrication of nanophotonic devices and circuits [5].

When the dimension of metal nanoparticles is small enough compared to the wavelength of the incident light, surface plasmon can be excited due to a collective motion of free electrons in the metal nanoparticles that resonantly couples with the oscillating electric field of the light. As a result of surface plasmon excitation, strong enhancement of the absorption, scattering, and local electric field around the metal particles arise and these feature strongly depends on particle size, shape, type of materials, and the local environment. As any change in the shape of the metal nanoparticles affect the pattern in which the free electrons are oscillating, the resonant frequency will change [6]. Though changing the size of spherical particles can induce smaller shift in the SPR peak position, in theory and in practice, changing the shape of silver nanoparticles provide more versatility. Anisotropic silver nanoparticles can absorb and scatter light along multiple axes. It is well known that the optical absorption spectra of silver nanorods and nanodisks are different from nanospheres. As

P. Sarkar · D. K. Bhui · H. Bar · G. P. Sahoo · S. Samanta ·
S. Pyne · A. Misra (✉)
Department of Chemistry and Chemical Technology, Vidyasagar
University, Midnapore 721 102, West Bengal, India
e-mail: ajaymsr@yahoo.co.in

spherical particles have strong SPR band at ~ 400 nm, while Ag nanorods usually show a red-shifted long-axis resonance (longitudinal plasmon band) and a slightly blue-shifted short-axis resonance (transverse plasmon band); and on the other hand, Ag nanodiscs have several resonance modes in the absorption spectra: (1) dipolar in-plane resonance, (2) dipolar out-of-plane resonance located; (3) quadrupolar out-of-plane resonance.

Much effort has been devoted to synthesize silver nanoparticles having various size and shapes. This includes zero-dimensional (0-D) spherical or tetrahedral quantum dots [7–9], one-dimensional (1-D) silver nanorods and wires [10, 11] and two-dimensional (2-D) nanoplates [12], nanoprisms [13] and nanodiscs [14, 15]. Synthesis of nanostructures via simple wet-chemical method is one of the most favoured routes towards the cost-effective large-scale production of nanobuilding blocks. Chemical synthesis of metal nanoparticles involves the reduction of metal salts followed by nucleation and growth in presence of stabilizing agents such as polymers [16, 17], thiols [18], CTAB [19], Na-AOT [20], SDS [21], unsaturated dicarboxylates [22], and plant extracts [23, 24]. More recently, the use of seeds to make more monodisperse metal nanoparticles along with various morphologies has been reported by various authors. Murphy and co-workers first reported the growth of citrate-stabilized gold nanoparticles by the seed-mediated method using a wide range of reducing agents and conditions [11, 25]. Using the same approach, they were able to prepare gold nanorods with tunable aspect ratios [26].

Synthesis of anisotropic metal nanoparticles motivates the development and innovation of theoretical methods for describing the unique properties of these nanoparticles. The study of colours of metal nanoparticles can be traced back to 19th century when Michael Faraday studied the colour of gold colloid in stained glass windows [27]. Mie presented an analytical solution to Maxwell's equations that describe an isolated spherical particle in 1908 [28]. Although many extensions of Mie theory have been made for covering different aspects including magnetic and coated spheres [29, 30], this analytical method has a fundamental limitation that the exact solutions are restricted only to highly symmetric particles such as spheres and spheroids. Recently, a number of theoretical approaches have been developed, based on more advanced scattering theories for anisotropic metal nanoparticles. These include the generalized multipole technique (GMT) [31], the T-matrix method [32], the discrete dipole approximation (DDA) [33], and the finite difference time domain (FDTD) method [34]. The first two methods can be classified as surface-based methods where only the particle's surface is discretized and solved numerically. The latter methods are referred to as volume-based methods where the entire volume is discretized. Among these methods, DDA has

been demonstrated to be one of the most powerful and flexible electrodynamics methods for computing the optical spectra of particles with an arbitrary geometry. DDA involves replacing each particle by an assembly of finite cubical elements, each of which is small enough that only dipole interactions with an applied electromagnetic field and with induced fields in other elements need to be considered. This reduces the solution of Maxwell's equation to an algebraic problem involving many coupled dipoles. The DDA method has been widely used to describe the shape dependence of plasmon resonance spectra, including studies of triangular prism [35], discs [36], cubes [37], truncated tetrahedral [38], shell-shaped particles [39], small clusters of particles [40], and many others [41]. Recently, Schatz group [42] has carried out extensive studies showing that DDA is suited for optical calculations of the extinction spectrum and the local electric field distribution in metal particles with different geometries and environments. Again, Lee and El-Sayed [43] have investigated the systematic dependence of nanorod absorption and scattering on their aspect ratio, size, and medium refractive index using DDA simulation method.

This article focuses on the synthesis of silver nanostructures of different morphologies via seeding growth approach, using methyl cellulose (MC) polymer as soft-template in the growth solution. It is shown that the concentration variation of tri-sodium citrate in the growth solution plays important role in controlling the morphology of the nanoparticles. We also represent the theoretical calculations of the extinction efficiency for nanospheres, nanodisks, and nanorods using discrete dipole approximation (DDA) methodology.

Experimental Section

Materials

Silver nitrate (AgNO_3 , >99%) and sodium borohydride (NaBH_4 , >99%) were purchased from S.D. Fine-Chem Ltd. Ascorbic acid and methyl cellulose (MC, 4000 cps, viscosity 2% (w/v), water, 20°C) were supplied by Merck India Ltd. Trisodium citrate was supplied by BDH Chemicals. Glassware was first rinsed with aqua regia and then washed thoroughly by triple distilled water before use. All solutions were prepared in triple distilled de-ionized water.

Synthetic Methods

(a) Synthesis of Silver Seeds

Typically, 20 mL aqueous solution containing 2.5×10^{-4} M AgNO_3 and 2.5×10^{-4} M tri-sodium citrate was

taken in a two-necked round bottom flask and stirred under ice-cold condition. Freshly prepared 0.1 M aqueous NaBH₄ (0.6 mL) solution was added dropwise to this mixture under vigorous stirring. The colour of the solution turned bright yellow immediately due to formation of silver colloid. This solution was kept in the dark and aged for 2 h prior to use as seed in the growth solutions.

(b) Synthesis of Silver Nanostructures of Different Morphologies

Growth solution was prepared by mixing 10 mL aqueous solution of MC (0.5 wt%), 0.3 mL tri-sodium citrate (1 mM), 0.1 mL ascorbic acid (0.1 M) and 0.15 mL silver nitrate (0.01 M) in a conical flask; 0.1 mL seed was added slowly with vigorous stirring to the above growth solution. Colour of the solution was changed gradually from colourless to yellow to red to green. Silver sols of different colour were also prepared by changing the concentration of citrate in the growth solution. Red-coloured silver sol was obtained by adding 0.3 mM tri-sodium citrate in the growth solution.

Instrumentations and Measurements

UV-vis spectroscopic study of silver colloids was done using a ‘SHIMADZU’ UV-1601 spectrophotometer. TEM and Energy-dispersive X-ray spectroscopy (EDX) study of Ag nanoparticles was carried out using JEOL-JEM-2100 high resolution transmission electron microscope (HR-TEM). Samples for the TEM and EDX studies were prepared by placing a drop of the aqueous suspension of particles on carbon-coated copper grids followed by solvent evaporation under vacuum.

Discrete Dipole Approximation

DDA is a numerical method in which the object studied is represented as a cubic lattice of N-polarizable point dipoles localized at $\mathbf{r}_j, j = 1, 2, \dots, N$, each one characterized by a polarizability α_j . There is no restriction on the localization of cubic lattice sites so that DDA represents a particle of arbitrary shape and composition. Polarization of each dipole, \mathbf{P}_j , is then described under the electric field at the respective position by

$$\mathbf{P}_j = \alpha_j \mathbf{E}_{\text{loc}}(\mathbf{r}_j) \quad (1)$$

where \mathbf{E}_{loc} is the electric field at \mathbf{r}_j that is the sum of the incident field $\mathbf{E}_{\text{inc},j}$ and the field radiated by all other N-1 induced dipoles $\mathbf{E}_{\text{other},j}$. The incident field $\mathbf{E}_{\text{inc},j}$ is given by

$$\mathbf{E}_{\text{inc},j} = \mathbf{E}_0 \exp(i\mathbf{k} \cdot \mathbf{r}_j - i\omega t) \quad (2)$$

where, \mathbf{r}_j is the position vector, t is the time, ω and \mathbf{k} are the angular frequency and the wave vector, respectively. The local field at each dipole is then represented by

$$\begin{aligned} \mathbf{E}_{\text{loc},j} &= \mathbf{E}_{\text{inc},j} + \mathbf{E}_{\text{other},j} \\ &= \mathbf{E}_0 \exp(i\mathbf{k} \cdot \mathbf{r}_j - i\omega t) - \sum_{j \neq k} \mathbf{A}_{jk} \cdot \mathbf{P}_k \end{aligned} \quad (3)$$

where \mathbf{P}_j is the dipole moment of the j th element and $-\mathbf{A}_{jk}\mathbf{P}_k$ is the electric field at including retardation effects. Each element \mathbf{A}_{jk} is a $3N \times 3N$ matrix which represents the interaction between all dipoles as given below:

$$\begin{aligned} \mathbf{A}_{jk} \cdot \mathbf{P}_k &= \frac{\exp(ikr_{jk})}{r_{jk}^3} \times \left\{ k^2 \mathbf{r}_{jk} \times (\mathbf{r}_{jk} \times \mathbf{P}_k) \times \frac{1 - ikr_{jk}}{r_{jk}^2} \right. \\ &\quad \times \left. \left[r_{jk}^2 \mathbf{P}_k - 3\mathbf{r}_{jk}(\mathbf{r}_{jk} \cdot \mathbf{P}_k) \right] \right\}, (j \neq k) \end{aligned} \quad (4)$$

where $\mathbf{r}_{jk} = \mathbf{r}_j - \mathbf{r}_k$ and $k = ||\mathbf{k}||$. Defining $A_{jj} = \alpha_j^{-1}$ reduces the scattering problem to finding the polarization \mathbf{P}_k that satisfy a system of N inhomogeneous linear complex vector equations.

$$\sum_{k=1}^N \mathbf{A}_{jk} \mathbf{P}_k = \mathbf{E}_{\text{loc},j}. \quad (5)$$

Once, Eq. 5 has been solved for the unknown polarizations \mathbf{P}_j , the extinction C_{ext} , absorption C_{abs} and scattering C_{sca} cross-sections may be evaluated from the optical theorem, thus giving

$$C_{\text{ext}} = \frac{4\pi k}{|\mathbf{E}_0|^2} \sum_{j=1}^N \text{Im}(\mathbf{E}_{\text{loc},j}^* \cdot \mathbf{P}_j) \quad (6)$$

$$C_{\text{abs}} = \frac{4\pi k}{|\mathbf{E}_0|^2} \sum_{j=1}^N \left\{ \text{Im}[\mathbf{P}_j \cdot (\alpha_j^{-1})^* \mathbf{P}_j^*] - \frac{2}{3} k^3 |\mathbf{P}_j|^2 \right\} \quad (7)$$

where the superscript asterisk denotes the complex conjugate. The scattering cross-section $C_{\text{sca}} = C_{\text{ext}} - C_{\text{abs}}$ may also be directly evaluated once the polarization \mathbf{P}_j is known. The target particle in the surrounding dielectric medium is considered by using a dielectric function of the target ϵ relative to that of the medium ϵ_m , which is reflected in the DDA calculation in the form of dipole polarizability. The dielectric function of silver is generated from the bulk experimental data of Johnson and Christy [44] and the medium is assumed to have a refractive index n_m of 1.34, close to that of the water.

The complex linear Eq. 5 for the induced polarization is solved by using the DDSCAT 7.0 program written by Drain and Flatau [45].

Results and Discussion

HR-TEM Study

Figure 1a shows the HR-TEM micrograph of silver seeds. Particles are mostly spherical in shape with diameter ranging between 3 and 5 nm. Particle size distribution histograms of silver seeds are given in Fig. 2a. HR-TEM micrograph (Fig. 1b) of the red coloured silver sol, obtained by using 0.3 mM of sodium citrate, shows that the particles are mostly circular disc like in shape. The TEM image suggests the presence of mostly nanodiscs, having diameter between 40 and 65 nm, with a very few number of spheres. The histogram of nanodisks distribution (Fig. 2b) shows that majority of discs have a diameter of \sim 55 nm. On the other hand, HR-TEM photograph of green-coloured silver sol (Fig. 1c), obtained by using 1 mM of sodium citrate, shows the presence of only silver nanorods of different aspect ratios ($R = 3\text{--}7$).

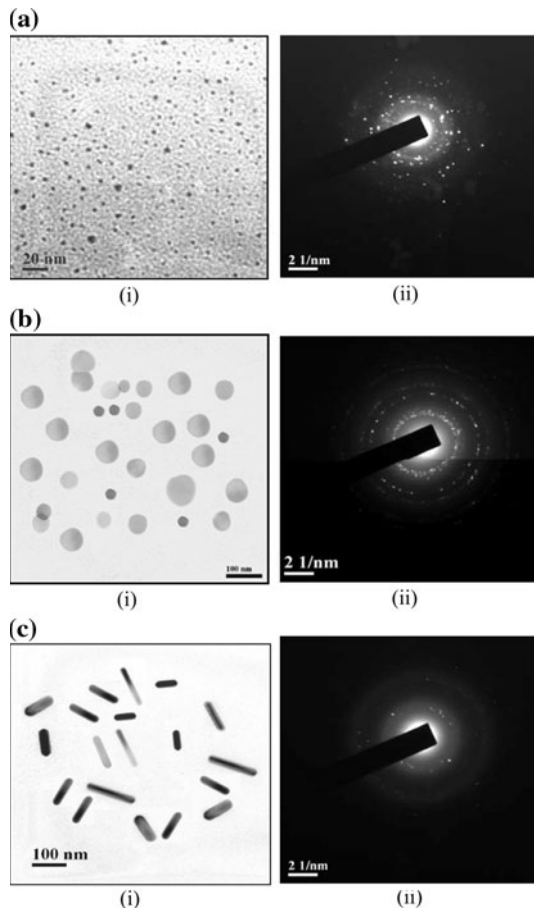


Fig. 1 a (i) High resolution transmission electron micrograph (HR-TEM) of silver seed solution and (ii) SAED pattern of nanoparticles, b (i) HR-TEM of red-coloured silver sol and (ii) SAED pattern of the corresponding sol and c (i) HR-TEM of green-coloured silver sol and (ii) SAED pattern of green sol

The histogram of particle distribution of corresponding silver nanorods (Fig. 2c) shows that majority of particles have aspect ratio of 4.

The selected area electron distribution pattern (Fig. 1a(ii), 1b(ii), 1c(ii)) shows concentric ring with intermittent bright dots, indicating that the samples are highly crystalline in nature. A closer look on the SAED pattern of Fig. 1b(ii) suggests that the ring having d -values 2.50, 1.227, 1.451, and 2.093 Å corresponds 1/3(422), (311), (220), and (200) crystal plane of fcc silver lattice. The set of spots with lattice spacing of \sim 2.50 Å is believed to originate from 1/3(422) plane normally forbidden by an fcc lattice. The appearance of the forbidden 1/3(422) plane is often observed on silver or

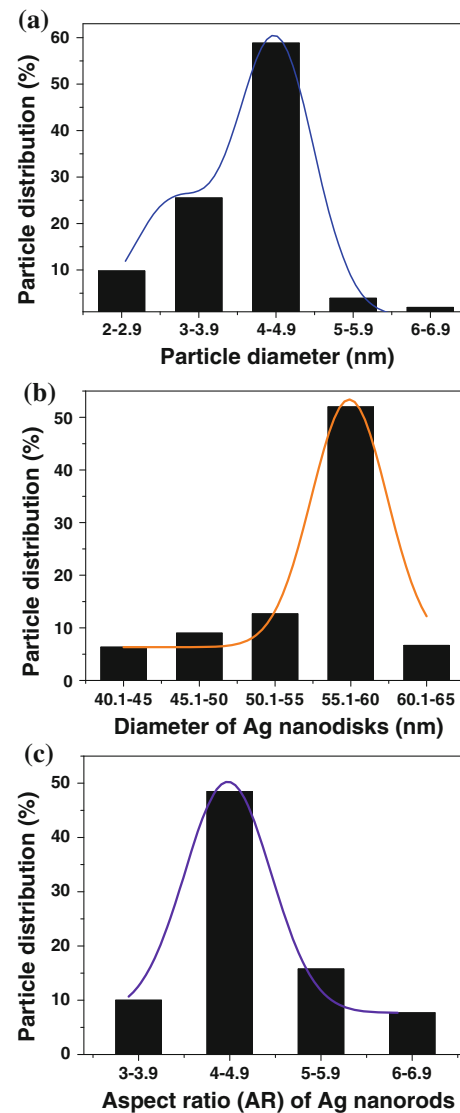


Fig. 2 Histogram distribution of a silver seeds, b silver nanodisks and c silver nanorods obtained from HR-TEM micrographs

gold nanostructures in the form of thin plate or film bound by atomically flat and bottom faces [46–50].

UV-vis Spectroscopy Study

It has been observed that silver nanoparticles of different morphologies can be synthesized using seed-mediated growth approach where the microfibril of methyl cellulose (MC) acts as soft-template for the growing particles. Formation of silver nanoparticles has been traced on-line by UV-vis spectra. Noble metal nanoparticles display localized surface plasmon resonance bands (LSPR) in the UV-vis region when the incident light resonates with the conduction band electrons on their surfaces [51]. The optical properties of silver nanoparticles are the most interesting because their UV-vis absorption spectrum is dominated by a very intense and narrow absorption band in the near UV and visible region. It is well known that the optical properties of metal nanoparticles depend strongly on the size, shape, interaction between the particles, and the absorbed species on the surface of the nanoparticles.

Figure 3b shows the surface plasmon resonance (SPR) extinction spectra of citrate-stabilized silver seeds. The yellow-coloured silver seeds sol displays sharp and intense SPR band at $\lambda_{\text{max}} = 398 \text{ nm}$. The observed absorption peak at around 398 nm is generally attributed to the surface plasmon resonance absorption of silver nanoparticles. UV-vis extinction spectra (Fig. 4a) of red-coloured silver sols exhibits three distinct plasmon absorption peaks in the spectrum located at ~ 340 , ~ 420 , and $\sim 665 \text{ nm}$. The peak at $\sim 340 \text{ nm}$ is attributed to the out-of-plane quadrupole resonance. The second peak at $\sim 420 \text{ nm}$ is normally attributed to the out-of-plane dipole resonance of nanodiscs and its relative intensity is much stronger than

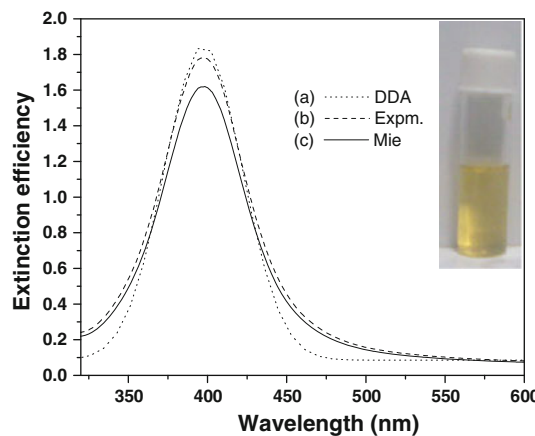


Fig. 3 Comparison of the extinction efficiency between experimental and theoretically simulated extinction spectra (both by Mie's theory and DDA method) of spherical silver particle (radius $\sim 4 \text{ nm}$). (Inset shows the photograph of silver seeds hydrogel)

that was theoretically expected [46]. Since spherical silver particles may also have their absorption band in this region, it suggests the existence of few spherical particles in the solution. The third peak at $\sim 665 \text{ nm}$ is due to in-plane dipole resonance of silver particles. This peak is very sensitive to the size of the nanodiscs and it is shifted to the red with the increased disc size.

UV-vis extinction spectra of green-coloured silver sols (Fig. 5a) show three distinct plasmon absorption bands in the spectrum located at ~ 800 , ~ 420 , and $\sim 330 \text{ nm}$. The band at $\sim 330 \text{ nm}$ is attributed to the out-of-plane quadrupole resonance. The band at ~ 800 and $\sim 420 \text{ nm}$ are due to in-plane dipole resonance (longitudinal) and out-of-plane dipole resonance (transverse) of silver nanorods.

Simulation of UV-vis Extinction Spectra Using DDA Method

We carry out the analytical calculations for SPR transition of silver nanosphere using the modified Mie's equation by Bohren and Hoffman equation [52] and compared the results with the convergent solution of DDA. Figure 3 shows the extinction efficiency factors, $Q_{\text{ext}}(\lambda) = C_{\text{ext}}(\lambda)/(\pi a^2)$, of silver sphere, having radius of $\sim 4 \text{ nm}$, both

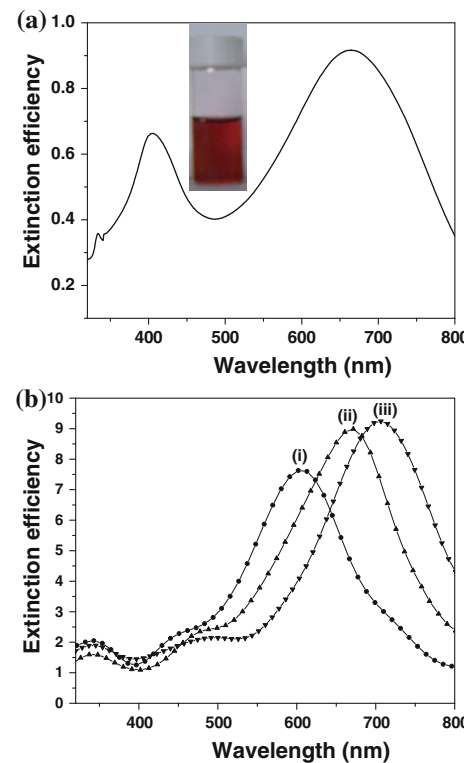


Fig. 4 **a** Experimental UV-vis extinction spectra of methyl cellulose (MC)-stabilized silver nanodisks. (Inset shows the colour of the corresponding sols) **b** DDA-simulated extinction spectra of silver nanodisks having different diameter (D)—(i) $D = 40$, (ii) $D = 50$ & (iii) $D = 60$

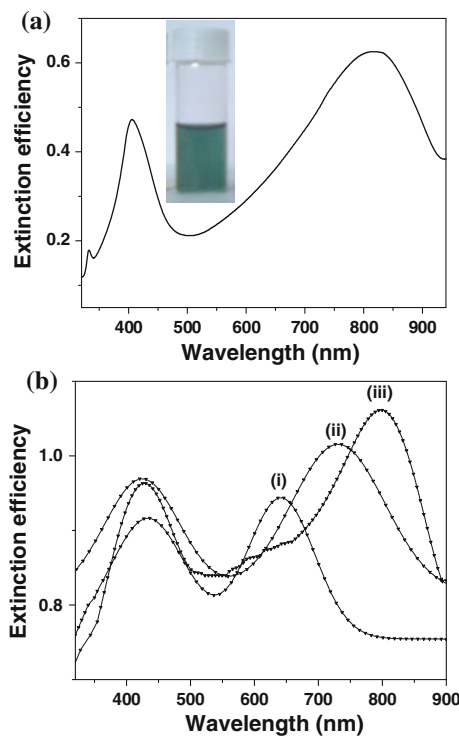


Fig. 5 **a** Experimental UV-vis extinction spectra of methyl cellulose (MC)-stabilized silver nanorods. (*Inset* shows the colour of the corresponding sols) **b** DDA-simulated extinction spectra of silver nanorods having different aspect ratios (R)—(i) $R = 3$, (ii) $R = 4$, & (iii) $R = 5$

experimentally and also theoretically calculated by using the modified Mie scattering theory and the DDA methodology. In these calculations, the refractive index of the surrounding medium is approximated to have a value of 1.34 at all wavelengths, close to that of water. Figure 3 illustrates that the DDA calculations are almost in good agreement with the results of the Mie scattering theory and also to that of the results obtained from experiments.

Theoretical calculation of extinction efficiency of both circular silver nanodiscs and nanorods are performed using DDA methodology. For this calculation, we adapt the DDSCAT 7.0 code developed by Drain and Flatau [45]. The disc absorbs and scatters light more strongly because its circular symmetry gives it a larger effective dipole moment [53]. Several resonance modes can be taken into account in the absorption spectra of silver nanodiscs: (1) dipolar in-plane resonance, the most studied resonance and located in the wavelength range between 600 and 1,000 nm; (2) dipolar out-of-plane resonance located around 400–600 nm; (3) quadrupolar out-of-plane resonance located around 340 nm. The position as well as intensity of all these resonances varies as a function of the nanodisc size. Effect of size on the optical scattering and absorption efficiencies and their relative contributions to the total extinction are systematically investigated for Ag

nanodiscs. HR-TEM micrograph (Fig. 1b) shows that the diameter of silver nanodiscs varies from 40 to 65 nm. Accordingly, we simulate the extinction spectra of nanodiscs using diameter 40, 50, and 60 nm and the simulated spectra are shown in Fig. 4b. From the Fig. 4b, it is obvious that as diameter increases, the in-plane-dipole plasmon resonance is gradually shifted to the red. For the Ag disc, the induced polarizations lead to three peaks that quantitatively match the experimental results shown in Fig. 4a. A comparison of Fig. 4a and b suggests that the sum of our simulated spectra(Fig. 4b-(i), (ii) & (iii)) will be much closer to the in-plane dipolar resonance band of our experimental spectra.

Simulation of SPR extinction spectra of silver nanorods is being done with fixed target orientation, where the propagation direction of the incident light is assumed to be perpendicular to the optic axis of the nanorod. Two orthogonal polarizations of incident light are being considered in the calculation, one with an electric field parallel to the optic axis and another that is perpendicular to it. The silver nanorod is considered to have geometry of a cylinder capped with two hemispheres. In case of nanorods, an important size variable parameter is the aspect ratio (R), i.e. the ratio of the nanorod dimension along the long axis to that of the short axis. Effect of aspect ratio on the optical scattering and absorption efficiencies and their relative contributions to the total extinction were systematically investigated. HR-TEM micrograph (Fig. 1c) shows that the aspect ratio of our synthesized silver nanorods is in the range from 3 to 6. Accordingly, we simulate the extinction spectra of nanorod using aspect ratio 3, 4, and 5 and the simulated spectra are shown in Fig. 5b. In addition to the surface plasmon band at ~ 420 nm, silver nanorods possess a band at longer wavelengths due to the surface plasmon oscillation along the long-axis of the nanorods, known as longitudinal plasmon band. From Fig. 5b, it is obvious that as the aspect ratio increases, the longitudinal plasmon band is gradually shifted to the red. A comparison of Fig. 5a and b suggests that sum of our simulated spectra (Fig. 5b-(i), (ii),(iii)) will be much closer to the in-plane dipolar resonance band of our experimental UV-vis extinction spectra.

Stabilization of Ag Nanoparticles

The citrate-stabilized silver seeds were prepared using sodium borohydride as a reducing agent under ice-cold condition. The as-prepared seed solution were then added to an aqueous growth solution containing methyl cellulose (0.5 wt%), tri-sodium citrate (1 mM), ascorbic acid (0.1 M), and silver nitrate (0.01 M). Ascorbic acid, a mild reducing agent, was used because of its ability to

precipitate metallic silver in acidic condition according to the following reaction-



Since anisotropic nanostructures are only favourable in a slow reduction process, we have used mild reducing agent, sodium citrate, during the growth process. It is shown that the concentration of additional tri-sodium citrate plays important role in controlling the morphology of the nanoparticles. The polyhydroxylated MC shows dynamic supramolecular association helped by intra and intermolecular hydrogen bond forming molecular level pools, which act as template for nanoparticle growth [54]. It is well known that the aqueous solution of MC contains size-confined, nano sized pools of inter-molecular origin [55]. The as-prepared silver nanoparticles are adsorbed within the hydrophobic part of MC layers, during the growth process.

The above seed-mediated method describes the preparation of silver sols whose colour as well as morphology can be tuned by varying the concentration of tri-sodium citrate in the growth (Scheme 1) solution. The seed particles consist of a mixture of single crystal and twinned crystals. HR-TEM analysis of the green sols shows the presence of only nanorods of different aspect ratios; on the other hand, the HR-TEM image of red-coloured silver sols suggests the presence of mostly nanodisks, having diameter ranging between 40 and 65 nm, with a very few number of spheres. The smaller spherical particles are formed in the growth process as single crystal seeds grow isotropically. On the other hand, twinned seed crystals grow

anisotropically in the presence of tri-sodium citrate to form disc and rod-shaped particles. It has been observed that the concentration of tri-sodium citrate in the growth solution has a major contribution in determining the morphologies of the nanoparticles, though the mechanism responsible at the molecular level is yet to be understood.

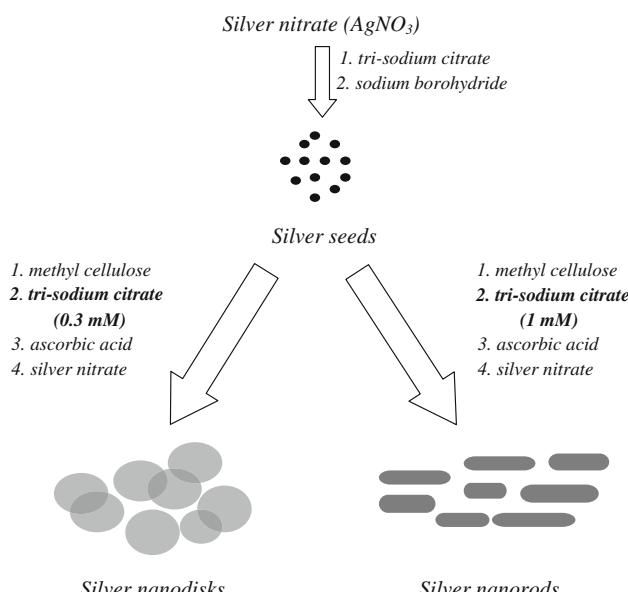
Conclusions

We present a simple seeding growth approach to synthesize silver nanostructure of different morphologies e.g. circular disc and rod-shaped particles. It has been observed that the colour of silver sols or to say the morphology of particles can be tuned by changing the concentration of tri-sodium citrate in the growth solution. Both the disc and rod-shaped silver nanoparticles exhibit interesting optical features. These optical extinction spectra are simulated theoretically using DDA-based computational methodology. Also, the accuracy and validity of the DDA calculations were verified by comparing the results with the well-known exact analytical solutions of Maxwell's equation using modified Mie theory for a sphere. A comparison of experimental and theoretical results has been made to elucidate the optical properties of both silver nanodisks and nanorods, synthesized by the above seeding growth approach. Our present simulation of extinction spectra using DDA calculation suggests the potentiality of DDA methodology while calculating the extinction spectra of anisotropically grown silver particles.

Acknowledgments We thank to Prof. S. Pati, Jawaharlal Nehru Centre for Advanced Scientific Research (JNCASR) Bangalore, India for helpful suggestions while doing the theoretical calculation using DDA method. P.S and S.P thanks to CSIR, New Delhi, for financial support. The support rendered by the Sophisticated Central Research Facility at IIT Kharagpur, India for sample analysis using HRTEM is gratefully acknowledged.

Open Access This article is distributed under the terms of the Creative Commons Attribution Noncommercial License which permits any noncommercial use, distribution, and reproduction in any medium, provided the original author(s) and source are credited.

References



Scheme 1 Schematic presentation of synthesis of silver nanodisks and nanorods using different citrate concentration through seed-mediated growth process

- B. Wiley, S. Im, Z. Li, J.M. McLellan, A. Siekkinen, Y. Xia, *J. Phys. Chem. B* **110**, 15666 (2006)
- A.D. McFarland, M.A. Young, J.A. Dieringer, R.P. Van Duyne, *J. Phys. Chem. B* **109**, 11279 (2005)
- P. Bharadwaj, P. Anger, L. Novotny, *Nanotechnology* **18**, 044017 (2007)
- J. Zhao, X. Zhang, C.R. Yonzon, A.J. Haes, R.P. Van Duyne, *Nanomedicine* **1**, 219 (2006)
- E. Ozbay, *Science* **311**, 189 (2006)
- U. Kreibig, M. Vollmer, *Optical properties of metal clusters*, vol. 25 (Springer, Berlin, 1995), p. 1995

7. A. Taleb, C. Petit, M.P. Pileni, *J. Phys. Chem. B* **102**, 2214 (1998)
8. A. Taleb, C. Petit, M.P. Pileni, *Chem. Mater.* **9**, 950 (1997)
9. S. Schneider, P. Halbig, H. Grau, U. Nickel, *Photochem. Photobiol.* **60**, 605 (1994)
10. Y. Sun, B. Gates, B. Mayers, Y. Xia, *Nano. Lett.* **2**, 165 (2002)
11. N.R. Jana, L. Gearheart, C.J. Murphy, *Chem. Commun.* **617** (2001)
12. A. Callegari, D. Tonti, M. Chergui, *Nano Lett.* **3**, 1565 (2003)
13. R. Jin, Y.C. Cao, E. Hao, G.S. Métraux, G.C. Schatz, C.A. Mirkin, *Nature* **425**, 487 (2003)
14. V. Germain, J. Li, D. Ingert, Z.L. Wang, M.P. Pileni, *J. Phys. Chem. B* **107**, 8717 (2003)
15. Y. Sun, Y. Xia, *Adv. Mater.* **15**, 695 (2003)
16. A.M. Whelan, M.E. Brennan, W.J. Blau, J.M. Kelly, *J. Nanosci. Nanotech.* **4**, 66 (2004)
17. C. Luo, Y. Zhang, X. Zeng, Y. Zeng, Y. Wang, *J. Coll. Int. Sci.* **288**, 444 (2005)
18. S. He, L. Yao, P. Jiang, D. Shi, H. Zhang, S. Xie, S. Pang, H. Gao, *Langmuir* **17**, 1571 (2001)
19. S. Chen, D.L. Carroll, *Nano. Lett.* **2**, 1003 (2002)
20. M. Maillard, S. Giorgio, M.P. Pileni, *J. Phys. Chem. B* **107**, 2466 (2003)
21. D.K. Bhui, P. Sarkar, H. Bar, G.P. Sahoo, S.P. De, A. Misra, *J. Mol. Liqs.* **145**, 33 (2009)
22. P. Sarkar, D.K. Bhui, H. Bar, G.P. SahooSarkar, S.P. De, A. Misra, *J. Lumin.* **129**, 704 (2009)
23. H. Bar, D.K. Bhui, G.P. Sahoo, P. Sarkar, S. Pyne, A. Misra, *Colloid. Surf. A* **339**, 134 (2009)
24. H. Bar, D.K. Bhui, G.P. Sahoo, P. Sarkar, S. Pyne, A. Misra, *Colloids Surf. A Physicochem. Eng. Aspects* **348**, 212 (2009)
25. N.R. Jana, L. Gearheart, C.J. Murphy, *J. Phys. Chem. B* **105**, 4065 (2001)
26. T.K. Sau, C.J. Murphy, *Langmuir* **20**, 6414 (2004)
27. M. Faraday, *Philos. Trans.* **147**, 145 (1857)
28. G. Mie, *Ann. Phys.* **25**, 377 (1908)
29. M. Kerker, D.S. Wang, C.L. Giles, *J. Opt. Soc. Am.* **73**, 765 (1983)
30. Z.S. Wu, Y.P. Wang, *Radio. Sci.* **26**, 1393 (1991)
31. A.C. Ludwig, *Comput. Phys. Commun.* **68**, 306 (1991)
32. M.I. Mishchenko, L.D. Travis, D.W. Mackowski, *J. Quant. Spectrosc. Radiat. Transfer.* **55**, 535 (1996)
33. B.T. Drain, P.J. Flatau, *J. Opt. Soc. Am. A* **111**, 1491 (1994)
34. J.P. Kottman, O.J.F. Martin, D.R. Smith, S. Schultz, *Opt. Express* **6**, 213 (2000)
35. L.J. Sherry, R. Jin, C.A. Mirkin, G.C. Schatz, R.P. Van Duyne, *Nano. Lett.* **6**, 2060 (2006)
36. L. Qin, S. Zou, C. Xue, A. Atkinson, G.C. Schatz, C.A. Mirkin, *Proc. Natl. Acad. Sci. USA* **103**, 13300 (2006)
37. L.J. Sherry, S.H. Chang, G.C. Schatz, R.P. Van Duyne, B.J. Wiley, Y. Xia, *Nano. Lett.* **5**, 2034 (2005)
38. A.J. Haes, J. Zhao, S. Zou, C.S. Own, L.D. Marks, G.C. Schatz, R.P. Van Duyne, *J. Phys. Chem. B* **109**, 11158 (2005)
39. E. Hao, S. Li, R.C. Bailey, S. Zou, G.C. Schatz, J.T. Hupp, *J. Phys. Chem. B* **108**, 1224 (2004)
40. E. Hao, G.C. Schatz, *J. Chem. Phys.* **120**, 357 (2004)
41. L. Zhao, S. Zou, E. Hao, G.C. Schatz, *Theor. Appl. Comput. Chem.* **47** (2005)
42. G.C. Schatz, *Theochem* **573**, 73 (2001)
43. A. Brioude, M.P. Pileni, *J. Phys. Chem. B* **109**, 23371 (2005)
44. P.B. Johnson, R.W. Christy, *Phys. Rev. B* **6**, 4370 (1972)
45. B.T. Draine, P.J. Flatau, User Guide for the Discrete Approximation Code DDSCAT 7.0. (2008), <http://arxiv.org/abs/0809.0337v4>
46. R.C. Jin, W. Cao, C.A. Markin, K.L. Kelly, G.C. Schatz, J.G. Zheng, *Science* **294**, 1901 (2001)
47. V. German, J. Li, D. Ingert, Z. Wang, M.P. Pileni, *J. Phys. Chem. B* **107**, 8717 (2003)
48. D.A. Genov, A.K. Sarychev, V.M. Shalaev, A. Wei, *Nano. Lett.* **4**, 153 (2004)
49. K. Imura, T. Nagahara, H.J. Okamoto, *J. Am. Chem. Soc.* **126**, 12730 (2004)
50. A. Wei, in *Nanoparticles: scaffolds and building blocks*, ed. by V.M. Rotello (Kluwer Academic, New York, 2004), pp. 173–200
51. P. Mulvaney, in *Nanoscale Materials in Chemistry*, ed. by K.J. Klabunde (Wiley, New York, 2001), p. 156
52. C.F. Bohren, D.R. Hoffman, *Absorption and scattering of light by small particles* (Wiley, New York, 1983)
53. J. Aizpurua, G.W. Bryant, L.J. Richter, F.J. Garcia de Abajo, B.K. Kelly, T. Mallouk, *Phys. Rev. B* **71**, 235420 (2005)
54. P. Raveendran, J. Fu, S.L. Wallen, *J. Am. Chem. Soc.* **12**, 13940 (2003)
55. A. Haque, E.R. Morris, *Carbohydr. Polym.* **22**, 161 (1993)